



AIAA 2003–0839

Computation of Prescribed Spin for a Rectangular Wing and for the F-15E Using Detached-Eddy Simulation

James R. Forsythe
Jonathan F. Wentzel

*Department of Aeronautics, United States Air Force Academy, CO
80840*

Kyle D. Squires

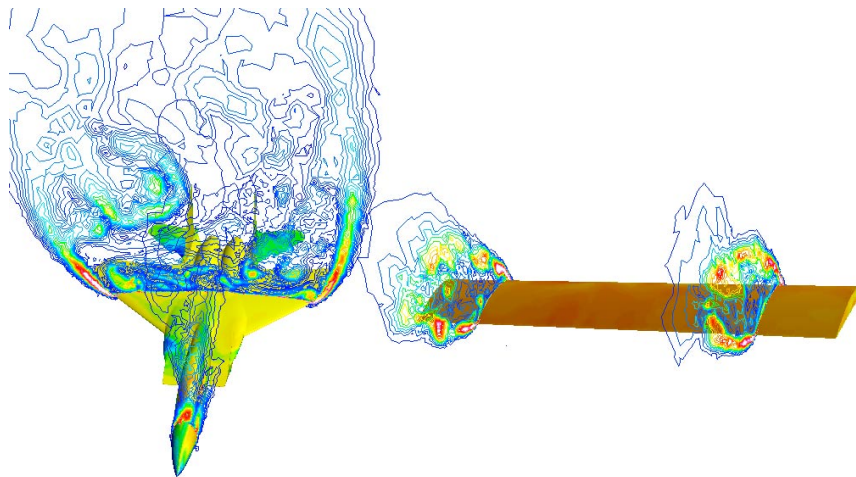
MAE Department, Arizona State University, Tempe, AZ 85287

Kenneth E. Wurtzler

Cobalt Solution, LLC, Miamisburg, OH 45459

Philippe R. Spalart

Boeing Commercial Airplanes, Seattle, WA 98124



41st Aerospace Sciences Meeting 6–9 January 2003 / Reno, Nevada

Computation of Prescribed Spin for a Rectangular Wing and for the F-15E Using Detached-Eddy Simulation

James R. Forsythe*

Jonathan F. Wentzel †

Department of Aeronautics, United States Air Force Academy, CO 80840

Kyle D. Squires‡

MAE Department, Arizona State University, Tempe, AZ 85287

Kenneth E. Wurtzler §

Cobalt Solution, LLC, Miamisburg, OH 45459

Philippe R. Spalart¶

Boeing Commercial Airplanes, Seattle, WA 98124

Detached-Eddy Simulation (DES) is used to predict the massively separated flow around a rectangular wing and around the F-15E statically, and then with prescribed spinning motions. The spinning motion of the rectangular wing is driven by the autorotative rolling moment of a wing just beyond stall, while that of the F-15E is triggered by a yawing moment, itself produced by asymmetric vortex shedding from the forebody even without spin. A drag polar for the static rectangular wing is produced using both RANS and DES. The two agree for attached flow; RANS then is more accurate near maximum lift, but DES is again more accurate post stall. Strip theory is applied to the drag polars to predict the limits of autorotative instability. The RANS polar shows only a weak susceptibility to autorotation over too-small an angle-of-attack range, while the DES polar closely matches the ranges based on experimental measurements. A prescribed rotary motion is then calculated using DES with the simulation predicting a pro-spin rolling moment, consistent with strip theory. In a parallel effort, a prescribed spin of the F-15E at 65° angle-of-attack is calculated by RANS and DES. Predictions are assessed via comparison to Boeing's stability and control database. A previous grid-resolution study leads to a 6.5×10^6 cell grid of the full aircraft with an efficient distribution of points. Although the grid is coarser than the baseline grid of the previous study, accurate force predictions are retained. A small bump is added to the nose of the aircraft that triggers the asymmetric vortex shedding on the forebody, as observed in flight and wind tunnel tests at this angle of attack. The yawing moment produced by the asymmetric vortices matches the database reasonably well. The accuracy in a prescribed spin is assessed by comparing the force coefficients with those for a static condition, with reference to the stability and control database. The effect of the rotation on lift and drag is captured adequately with RANS, but that on the yawing moment is not. DES does not yield similar effects, possibly because the expected change in lift and drag is quite small (less than 5%) and obscured by statistical fluctuations in a marginal time sample. Further grid refinement may also be required. Nevertheless, the overall force coefficients in the static case and prescribed spin are reasonably accurate and motivate a six-degree-of-freedom calculation in the near future.

Introduction

NUMERICAL simulation of the flow around complex configurations offers a powerful tool for analysis, e.g., a means to screen configurations prior to costly, hazardous and time-consuming flight tests. One example is spin testing in which Computational

Fluid Dynamics (CFD) could be used to provide detailed information on stability, spin modes, etc. Aircraft spin was discovered very early in the history of aviation. It was the cause of countless accidents from both unintentional entries and aerobatic stunts. Over time, pilots learned how to avoid and recover from spins, engineers learned to make the spins more benign or even impossible, and soon after its discovery spin testing became an integral part of flight testing. For many years now, spins have been a maneuver that is safely taught in many aviation schools. However, "the stall-spin is one of the major causes of light airplane

* Associate Professor, Senior Member AIAA

† Cadet, Student Member AIAA

‡ Professor, Member of AIAA

§ Vice President, Member of AIAA

¶ Senior Scientist

This paper is a work of the U.S. Government and is not subject to copyright protection in the United States.2003

accidents even today.”²³ If designers have a reliable tool to predict spin characteristics of different aircraft, aircraft can be designed to be more resistant to spin. Recovery steps can be demonstrated and optimized. A similar problem is the possible “tumble” of flying-wing aircraft, which could become a “show-stopper” in commercial applications (unless maybe absolute stall protection could be considered established through electronic limiters). None of today’s tools for such problems are based on a direct CFD solution of the flow.

Although flight testing is the best way to determine an aircraft’s spin characteristics, it cannot be used as a design tool since it requires a completed aircraft to test. Wind tunnel testing is often performed on working design models, but there are many inherent inadequacies stemming from wind tunnels, including issues of dynamic scaling and Reynolds number effects.²² There are also several analytical methods that have been used to predict spinning tendencies of aircraft. However, “the airplane spin is not very amenable for theoretical analysis because of nonlinear, inertial cross coupling between the longitudinal and lateral degrees of freedom. Furthermore, the aerodynamics of the spinning airplane are extremely complex because of extensive flow separation over the wing and tail surfaces.”²³

Computational Fluid Dynamics represents a new arena for spin research and engineering. It is far less costly than other forms of testing and it is usable in earlier phases of design. CFD also allows for a much deeper understanding of the airflow than either wind tunnel, flight, or analytical methods. However, spins represent the type of flow that historically has been very challenging for CFD to predict accurately. This is primarily due to the very large regions of separated, highly turbulent flow behind the aircraft that challenge current models. These separated regions also mediate the interference between separate control surfaces, notably the horizontal and vertical tails, which are known to have great control over spin.

Most current engineering approaches, even to the prediction of unsteady flows, are based on solution of the Reynolds-averaged Navier-Stokes (RANS) equations. The turbulence models employed in RANS methods, at first sight, parameterize the entire spectrum of turbulent motions; in practice some flow conditions “push” RANS solutions into unsteady behavior, typically with alternating vortex shedding. While often adequate in steady flows with no regions of flow reversal, or possibly exhibiting shallow separations, it appears inevitable that RANS turbulence models will be unable to accurately predict the phenomena dominating flows characterized by massive separations. Unsteady massively separated flows are characterized by geometry-dependent and three-dimensional turbulent eddies. These eddies, arguably, are what defeats

RANS turbulence models, of any complexity.

To overcome the deficiencies of RANS models for predicting massively separated flows, Spalart *et al.*² proposed Detached-Eddy Simulation (DES) with the objective of developing a numerically feasible and accurate approach combining the most favorable elements of RANS models and Large Eddy Simulation (LES). The primary advantage of DES is that it can be applied at high Reynolds numbers (as can Reynolds-averaged techniques) but also, grid permitting, resolves geometry-dependent, unsteady three-dimensional turbulent motions as in LES. Typically, LES behavior takes place outside the boundary layers. DES predictions to date have been favorable, forming one of the motivations for this research. The specific aims are to apply and assess DES, consistent with the long-term goal of developing a CFD tool for analysis and prediction of aircraft spin. The goal is to assess DES predictions against both measurements and predictions of the same configuration obtained using a RANS turbulence model.

In this contribution, static (non-moving) and prescribed rotary motions are computed on a rectangular wing, and on the F-15E. Since the motions are prescribed, inertial effects are not considered. Including the inertial effects will be a focus of future six degree-of-freedom calculations. These two cases are of value due to the different physics driving the spin. The rectangular wing is susceptible to autorotation post-stall. In a spinning motion, the downward going wing sees a larger effective angle of attack and a reduced resultant force. The upward going wing sees a lower angle of attack and an increased resultant force. This provides a pro-spin rolling moment that drives the spin even absent any disturbances. Since this phenomenon occurs just beyond maximum lift, the rectangular wing exhibits shallow spin characteristics, with roll being the primary mode of motion.

The spin of the F-15E (and many jet fighter aircraft), on the other hand, is driven by forebody aerodynamics. At high angles of attack the rounded forebody produces asymmetric vortices which produce a large yawing moment.²¹ Although this effect would not be expected for a symmetric body, it can be caused by extremely small disturbances near the tip of the forebody (such as paint chips or manufacturing imperfections), so it is always effectively present, even without sideslip. Because of the low aspect ratio of the F-15E and the strong yawing moment from the forebody, the aircraft spin is closer to flat, with yaw being the primary mode of motion.

The rectangular wing considered is based on the Göttingen 387-FB airfoil section due to the availability of autorotation tests.²⁰ The tests include full drag polars for the wing from $\alpha = -8^\circ$ to 90° . Strip theory was applied to the measured drag polar for the wing in order to predict the limits of rotary stabil-

ity. Subsequently, free-to-spin tests were performed to directly define the autorotation envelope, and to test the effectiveness of strip theory. The CFD calculations presented (RANS and DES) mirror this approach. First, a drag polar is built for the wing based on static (non-moving) calculations. Strip theory is applied to find the limits of rotary instability. Then a prescribed spinning motion is performed in the range in which autorotation is expected to see if the rolling moment predicted is pro-spin, or at least is neutral for some roll rate. Future efforts will include a single degree-of-freedom calculation to more closely mirror the experiments and define the autorotative envelope fully.

For the full aircraft, the current effort focuses on the F-15E because of the availability of an extensive stability and control database.¹ This database was compiled from an extensive series of flight tests, including spins. Gaps in the flight test were filled in with wind tunnel testing. The aircraft at 65° angle of attack is the primary focus of the study since it is the angle at which a clean F-15E will maintain a stable spin. Accuracy is assessed by comparing force and moment coefficients without motion, and with the prescribed spin provided by the database. Previous calculations²⁵ at this angle of attack explored grid resolution and timestep requirements, thus guiding the current effort.

For calculations of complex configurations at high Reynolds numbers, high-performance computation is essential. In this work, solutions of the compressible Navier-Stokes equations on unstructured grids are obtained using the commercial code Cobalt.³ The numerical method is based on a finite-volume approach and is second-order accurate in space and time. The method is point-implicit and permits CFL numbers as large as one million for steady-state computations.⁵ Turbulence-resolving simulations are necessarily time dependent, and for DES the code is run in a time-accurate fashion. The computations are performed in parallel using the Message Passing Interface.⁴

Computational Approach

Spalart-Allmaras Model

The Spalart-Allmaras (referred to as ‘S-A’ throughout) one-equation model⁶ solves a single partial differential equation for a variable $\tilde{\nu}$ which is related to the turbulent viscosity. The differential equation is derived by “using empiricism and arguments of dimensional analysis, Galilean invariance and selected dependence on the molecular viscosity.”⁶ The model includes a wall destruction term that reduces the turbulent viscosity in the log layer and laminar sublayer and trip terms that provides a smooth transition from laminar to turbulent flow. In the present computations, the trip term was not active, and the equation

was

$$\frac{D\tilde{\nu}}{Dt} = c_{b1}\tilde{S}\tilde{\nu} - c_{w1}f_w \left[\frac{\tilde{\nu}}{d} \right]^2 + \frac{1}{\sigma} \left[\nabla \cdot ((\nu + \tilde{\nu}) \nabla \tilde{\nu}) + c_{b2} (\nabla \tilde{\nu})^2 \right] \quad (1)$$

The turbulent viscosity is determined via,

$$\nu_t = \tilde{\nu} f_{v1}, \quad f_{v1} = \frac{\chi^3}{\chi^3 + c_{v1}^3}, \quad \chi \equiv \frac{\tilde{\nu}}{\nu}, \quad (2)$$

where ν is the molecular viscosity. Using S to denote the magnitude of the vorticity, the modified vorticity \tilde{S} is defined as,

$$\tilde{S} \equiv S + \frac{\tilde{\nu}}{\kappa^2 d^2} f_{v2}, \quad f_{v2} = 1 - \frac{\chi}{1 + \chi f_{v1}}, \quad (3)$$

where d is the distance to the closest wall. The wall destruction function, f_w is,

$$f_w = g \left[\frac{1 + c_{w3}^6}{g^6 + c_{w3}^6} \right]^{\frac{1}{6}} \quad (4)$$

$$g = r + c_{w2}(r^6 - r), \quad r \equiv \frac{\tilde{\nu}}{\tilde{S}\kappa^2 d^2}. \quad (5)$$

The closure coefficients are given by:

$$\begin{array}{lll} c_{b1} = 0.1355 & \sigma = 2/3 & c_{b2} = 0.622 \\ \kappa = 0.41 & c_{w1} = \frac{c_{b1}}{\kappa^2} + \frac{(1+c_{b2})}{\sigma} & c_{w2} = 0.3 \\ c_{w3} = 2 & c_{v1} = 7.1 & \end{array} \quad (6)$$

Detached-Eddy Simulation

The DES formulation in this study is based on a modification to the Spalart-Allmaras RANS model⁶ such that the model reduces to its RANS formulation near solid surfaces and to a subgrid model away from the wall.⁷ The basis is to attempt to take advantage of the usually adequate performance of RANS models in the thin shear layers where these models are calibrated and the power of LES for resolution of geometry-dependent and three-dimensional eddies. The DES formulation is obtained by replacing in the S-A model the distance to the nearest wall, d , by \tilde{d} , where \tilde{d} is defined as,

$$\tilde{d} \equiv \min(d, C_{DES}\Delta). \quad (7)$$

In Eqn. (7) for the current study, Δ is the largest distance between the cell center under consideration and the cell center of the neighbors (i.e., those cells sharing a face with the cell in question). In “natural” applications of DES, the wall-parallel grid spacings (e.g., streamwise and spanwise) are at least on the order of the boundary layer thickness and the S-A RANS model is retained throughout the boundary layer, i.e., $\tilde{d} = d$. Consequently, prediction of boundary layer separation

is determined in the ‘RANS mode’ of DES. Away from solid boundaries, the closure is a one-equation model for the SGS eddy viscosity. When the production and destruction terms of the model are balanced, the length scale $\tilde{d} = C_{DES}\Delta$ in the LES region yields a Smagorinsky scaling for the eddy viscosity $\tilde{\nu} \propto S\Delta^2$. Analogous to classical LES, the role of Δ is to allow the energy cascade down to the grid size; roughly, it makes the pseudo-Kolmogorov length scale, based on the eddy viscosity, proportional to the grid spacing. The additional model constant $C_{DES} = 0.65$ was set in homogeneous turbulence⁸ and is used without modification in this study.

Code Details

The computations were performed using using Cobalt₆₀³ and Cobalt. Cobalt is a commercial version of Cobalt₆₀ (a Navier-Stokes solver developed at the Air Force Research Laboratory). The improvements to the commercial version relevant to this study were the ability to compute time-averages and turbulent statistics, faster per-iteration times, an improved spatial operator, and improved temporal integration. Additionally, Cobalt is capable of computing geometries undergoing rigid body motion, a crucial feature required to spin the aircraft in subsequent simulations. The timestep study was performed using Cobalt₆₀, while the grid refinement study was performed using Cobalt.

Cobalt is an unstructured finite-volume method developed for solution of the compressible Navier-Stokes equations and described in Strang *et al.*³ The numerical method is a cell-centered finite volume approach applicable to arbitrary cell topologies (e.g, hexahedra, prisms, tetrahedra). The spatial operator uses the exact Riemann Solver of Gottlieb and Groth,⁹ least squares gradient calculations using QR factorization to provide second order accuracy in space, and TVD flux limiters to limit extremes at cell faces. A point implicit method using analytic first-order inviscid and viscous Jacobians is used for advancement of the discretized system. For time-accurate computations, a Newton sub-iteration scheme is employed, and the method is second order accurate in time.

For parallel performance, Cobalt uses the domain decomposition library ParMETIS¹⁰ to provide nearly perfect load balancing with a minimal surface interface between zones. Communication between processors is achieved using Message Passing Interface (MPI), with parallel efficiencies above 95% on as many as 1024 processors.⁴

Grid motion

Simulation of rigid-body motion is achieved through an Arbitrary Lagrangian Eulerian (ALE) formulation, where the grid is neither stationary nor follows the fluid motion. The conservation equations are solved in an inertial reference frame, but the spatial operator

is modified so that the advection terms are relative to the (non-inertial) grid reference frame. This requires simple modifications to many boundary conditions and to the initial conditions for the Riemann problem. The inviscid and viscous work terms due to the grid velocity must also be removed from the spatial operator. The ALE formulation also forces certain modifications to the time-centered implicit temporal operator. At the beginning of a time-step, all geometric quantities are transformed to their values at the end of the given time-step, according to the specified motion. This ensures the fluxes, which an implicit scheme computes at the end of the time-step, are consistent with the geometry. Such quantities include centroid locations and least-squares weights vectors, but since the motion is rigid, volume and area are invariant under the transformation. A number of Newton sub-iterations are used to reduce errors associated with integrating over the time-step with an implicit temporal operator. The method has been applied to a pitching prolate spheroid¹² and a spinning forebody¹³ with good agreement to experiments.

Rectangular Wing

Introduction

The primary focus of the calculation on the rectangular wing was to examine the effectiveness of DES coupled with grid motion to predict autorotation of a wing. Knight²⁰ defines the following terms concerning autorotation:

1. Stable Autorotation: A state of equilibrium of rotation in which after any disturbance the aircraft will return to rotation.
2. Unstable Autorotation: A state of equilibrium in which a pro-spin disturbance will cause stable autorotation and an opposing disturbance will cause the aircraft to cease rotation.
3. Rotary Instability: A state of motion without rotation in which any rotary disturbance will cause stable autorotation.
4. Rotary Stability: A state of motion without rotation in which any rotary disturbance will cause the aircraft to return to a state without rotation.

The autorotation characteristics of the Göttingen 387-FB airfoil was studied by Knight²⁰ by applying strip theory to wind tunnel polars as well as performing experiments where the model was free to rotate around the velocity vector. These experiments form the baseline for the current study.

Strip theory focuses on analyzing rotary instability and stability only. Although usually applied to 2-dimensional sectional coefficients, Knight²⁰ applied strip theory to the full wing drag polar with good comparison to his free to spin experiments in most cases.

As detailed by Knight²⁰ and Pamadi,²³ strip theory predicts that a rectangular wing will exhibit rotary instability if

$$\frac{dC_R}{d\alpha} < 0 \quad (8)$$

where $C_R = \sqrt{C_L^2 + C_D^2}$ is the resultant force coefficient. Thus, the limits of rotary instability can be predicted corresponding to the regions of the drag polar in which the resultant force coefficient is decreasing.

Knight²⁰ also performed free-to-spin wind tunnel tests around the velocity vector and the quarter chord and determined stability within rotation as well as rotary stability and instability. An initial rotation rate was provided to the model in order to determine for which angles of attack the rotation is sustained. A range of angles of attack were found where the model, despite having rotary stability, would autorotate if given a large enough starting rotation rate.

Calculation Details

A single unstructured grid consisting of 4×10^6 cells was generated using Gridgen (see Figure 1). A prism layer containing approximately 50% of the cells was grown from the surface of the wing. The rest of the grid was comprised of tetrahedra, and was clustered above the upper surface of the airfoil to provide LES resolution of the separated wake. During the runs, the average first y^+ value was less than 1. The size and scale of the wing were drawn consistent with the experimental setup — a rectangular wing with no twist and a Göttingen 387-FB airfoil section. The chord was five inches while the wingspan was 30 inches, giving an aspect ratio of 6.

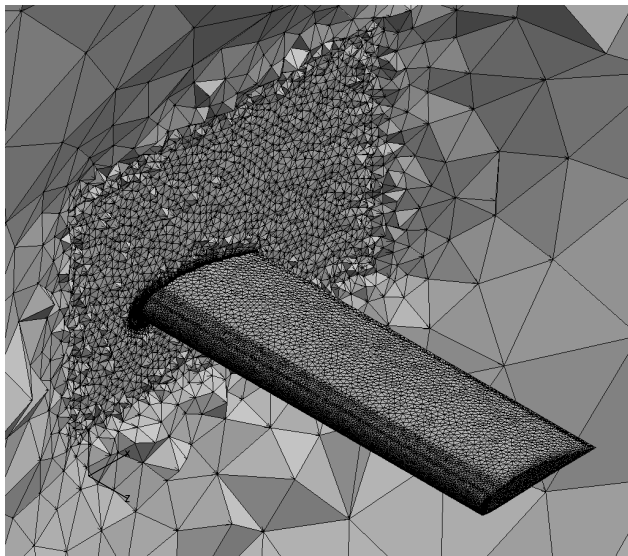


Fig. 1 View of the grid over the Göttingen 387-FB wing, with a cutting plane along the centerline.

The timestep used for the DES runs was 0.01 when non-dimensionalized by the chord and the freestream velocity, based on previous experience with DES airfoil

calculations. Time averages were taken after the first 2000 timesteps for an additional 4000 timesteps (40 non-dimensional time units) to provide time averaged lift and drag coefficients. This is a shorter temporal sample than employed by Shur *et al.*⁸ for an airfoil section (one chord into the span), however, the large aspect ratio of the wing in the current study leads to lower levels of oscillations in the forces, alleviating some of the error associated with lower sampling intervals. Nevertheless, additional sampling would reduce the uncertainty of the current calculations. Three Newton subiterations were used for the cases without motion, while five were used with the case with motion. For the RANS runs, a maximum CFL of 1×10^6 was used to accelerate the convergence to steady state.

The experimental Mach number (0.0524), and Reynolds number (153,000) were matched in the computations. Despite the low Reynolds number, the boundary layers were assumed fully turbulent in the computations. Use of trips in the experiments was not mentioned in Knight.²⁰ Wind tunnel walls were not modeled.

Results

Drag polars from the RANS and DES are plotted and compared to the experimental polar in Figure 2. Calculations were only performed up to 45° , since beyond that angle the experiments showed rotary stability. The DES and RANS predictions agree well with each other and the experiments at low angles. The boundary layer is attached for these cases, the DES model acting in its RANS mode yields essentially the same solution as the RANS over the wing. Discrepancy between the two solutions is apparent approaching $C_{L_{max}}$, with DES underpredicting the lift more significantly, though both techniques are below the maximum measured value. It should be noted that the CFD computations were performed at coarse intervals (12° , 18° , and 24°), making it likely that $C_{L_{max}}$ was not precisely identified in the computations (although it should have occurred at 18°). Post stall, DES is in closer agreement to the experiments, with RANS overpredicting the lift and drag by as much as 70%. This over-prediction by RANS at high angles of attack is analogous to that observe by Shur *et al.*⁸ on an airfoil section. The drop in lift is too gradual for the DES calculation, while it is virtually non-existent for the RANS.

To gain insight into the under-prediction near $C_{L_{max}}$ for DES, flow visualizations are shown at 18° , 24° and 45° in Figure 3. For the 18° case the wingtip vortices assist the flow in remaining attached near the wingtips. The separation near the centerline is relatively shallow, which places a larger burden on DES. This shallow separation constitutes a “grey area” for hybrid methods such as DES in which turbulent eddies may not rapidly develop following boundary layer

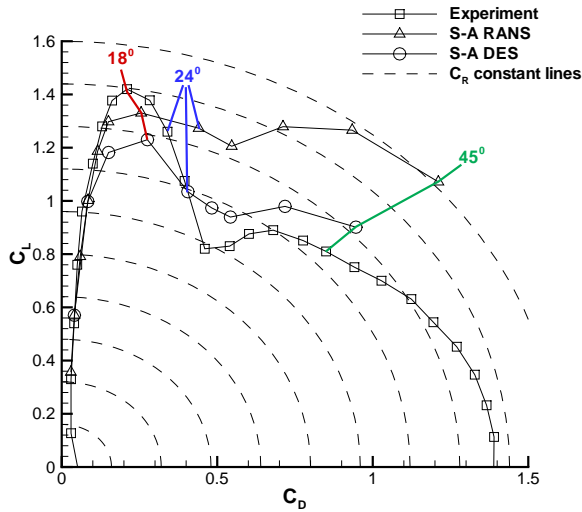
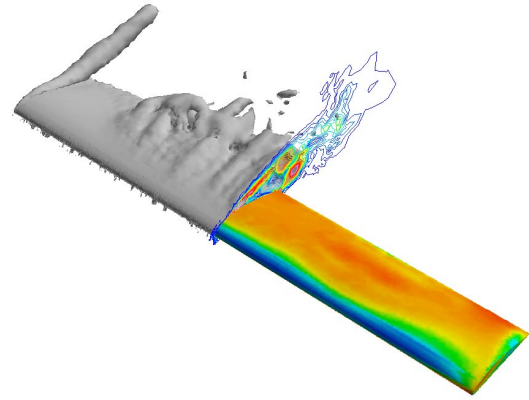


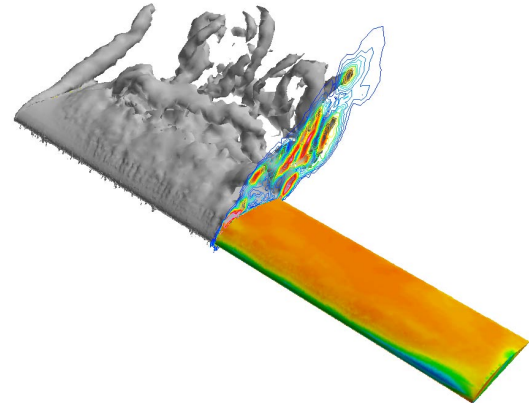
Fig. 2 Computed and Experimental²⁰ drag polar of the Göttingen 387-FB wing.

detachment. The Reynolds-averaged treatment suppresses substantial eddy content near solid surfaces, and the lack of structural features in the detaching boundary layers may contribute to more substantial errors in shallow separation prediction than in massively separated flows. From Figure 3(a) the shear layer separating off the centerline does not roll up until close to the trailing edge. Increased grid resolution could improve these results by lowering the model and numerical dissipation to allow for a more accurate LES treatment in the region. Forsythe and Woodson²⁴ applied adaptive mesh refinement to a DES prediction of shock separated flow on the F/A-18E, for example, and substantially improved the separation predictions at shallow angles of attack. Figure 3(b) shows the flow at $\alpha = 24^\circ$, which is in closer agreement to the experiments. The flow is now more massively separated with corresponding improved unsteady content in the separation bubble. Near the wing tips, however, the flow continues to exhibit shallow separation, stressing the model in that region. Figure 3(b) then shows the flow at $\alpha = 45^\circ$, which is massively separated over the entire wing. The grid resolution for this condition is sufficient to resolve numerous large scale eddies over the wing leading to the more accurate predictions of the lift and drag.

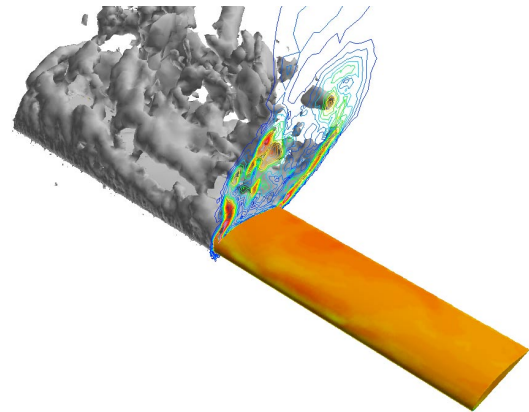
Despite these issues related to the current DES, they show a substantial improvement over the RANS calculations in the context of autorotation prediction. By inspecting Figure 2 with Equation 8 in mind, the RANS predictions predict only a weak autorotation tendency over a limited angle of attack range since the resultant force does not rapidly decrease post stall. DES, on the other hand, is in closer agreement to the experiments in predicting the rapid drop in the normal force. Quantitative aspects for the angle of attack



a) $\alpha = 18^\circ$



b) $\alpha = 24^\circ$



c) $\alpha = 45^\circ$

Fig. 3 Flow visualizations of DES of Göttingen 387-FB airfoil with no motion. Grey isosurface of vorticity, contours of vorticity on centerline, wing colored by pressure.

range where rotary instability is expected are obtained by examining $dC_R/d\alpha$ in Figure 4. These curves were obtained by applying a central difference approximation to the coefficients from the experiments and calculations. Since the drag polar from the computations was constructed using fewer points, the accuracy of instability limits should be lower compared to the range obtained using the experimentally determined values of the lift and drag. For the RANS calculations, only a narrow angle of attack range is expected to exhibit rotary instability. The DES predictions, on the other hand, compare closely to the experiments for the angle-of-attack range of rotary instability. The peak strength of the instability (which depends on $dC_R/d\alpha$), however, is under-predicted. This could in part be due to the lower number of angles treated in the simulations. The limits of rotary instability based on strip theory for the simulations and experiments are shown in Table 1. The actual limits of rotary stability as determined by the free-to-spin wind tunnel tests are also included showing the validity of strip theory (at least on this model).

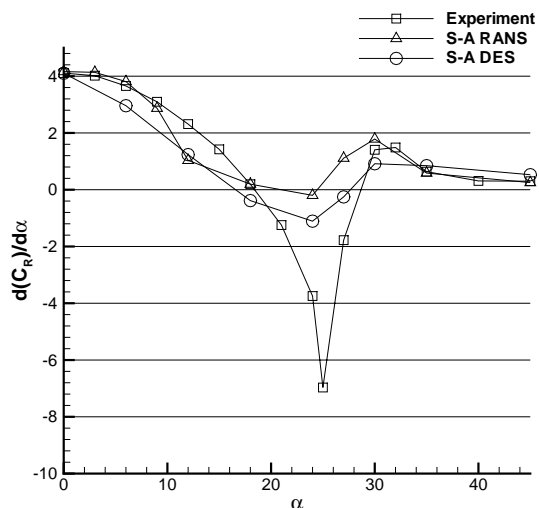


Fig. 4 Change in resultant force coefficient with angle-of-attack — Computed vs. Experimental.²⁰

	Lower Limit α ($^\circ$)	Upper Limit α ($^\circ$)
Experimental ²⁰	19.5	30.0
Exp, Strip Theory ²⁰	18.5	28.7
S-A DES, Strip Theory	16.5	27.5
S-A RANS, Strip Theory	21.0	24.5

Table 1 Limits of rotary instability for the Göttingen G387-FB wing.

Based on the partial success of DES in predicting the limits of rotary instability, a prescribed spin was attempted. Although all the experiments with motion were free-to-spin, this approach was taken to first con-

firm that a pro-spin moment could be generated with a small specified motion. Future efforts will use a single degree-of-freedom model to predict the rotation rates that were experimentally determined. The grid was rotated around the quarter chord (as with the experiments) with a small rate of rotation about the velocity vector with the right wing moving downward (as the pilot sits). The rotation rate specified gave an induced change in angle of attack of three degrees at the wing tip, i.e. $\Phi = \tan^{-1}(\Omega b/2U_\infty) = 3^\circ$, where Ω is the rotation rate, and b is the span. This low spin rate was chosen to keep the the effect on rolling moment within the linear range. The equilibrium spin rates from the experiments were much higher. The angle of attack chosen for testing was 24° , since it is expected to have the strongest autorotative effect.

A plot of rolling moment vs. time is shown in Figure 5. The motion was initiated abruptly from the end of a static case at $t=0.31$ sec. The startup motion gives an initial anti-spin rolling moment (negative). Then after the flow adjusts to the effect of the motion, the moment becomes pro-spin (positive), and remains pro-spin, although fluctuating. The cause of the pro spin moment is shown in Figure 6. The left wing (as the pilot sits) separates slightly later due to the reduced effective angle of attack as it moves up, giving a stronger lift than the right wing. Since the net moment is positive, a planned one degree-of-freedom calculation should predict an acceleration to a faster roll rate. Comparing the equilibrium roll rate to the experimental value should provide quantitative analysis of the accuracy of the computational method.

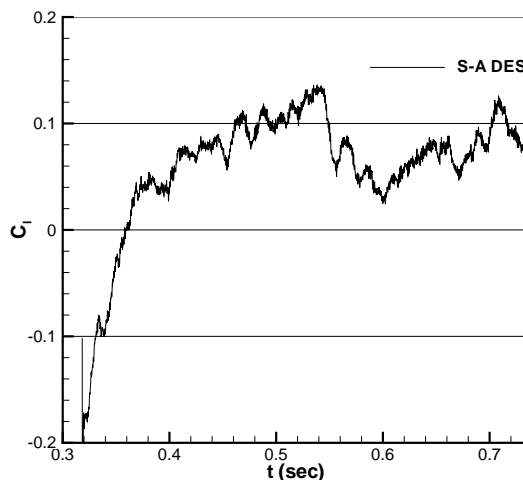


Fig. 5 Rolling moment vs. time for S-A DES of the Göttingen 387-FB wing in a prescribed spin at $\alpha = 24^\circ$

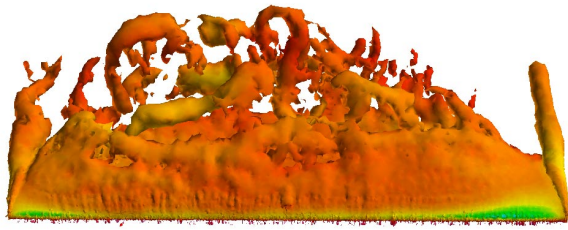


Fig. 6 Flow visualization of the prescribed spin of the Göttingen 387-FB wing using S-A DES at $\alpha = 24^\circ$. Isosurface of vorticity colored by pressure.

F-15E

Approach

The second prescribed spin attempted was of an F-15E at $\alpha = 65^\circ$ and $\beta = -2.5^\circ$. A stable spin was provided from the stability and control database¹ for a clean aircraft with a symmetric fuel load. The condition detailed the spin rate and the force and moment coefficients static and spinning. The spin was predicted from the database by an in-house code that predicted a spin state by balancing the force and moment coefficients with inertial forces and engine inertial effects. Since the current calculations employ specified motions, they do not account for the inertial forces or engine inertial effects. However if the force and moment coefficients predicted in the computations are close to the database values, then a force balance should be obtained. Future six degree-of-freedom calculations would directly predict the inertial effects.

Calculation Details

Forsythe *et al.*²⁵ performed a grid resolution study using VGRIDns¹⁵ on a half-aircraft model of the F-15E at $\alpha = 65^\circ$ and $\beta = 0^\circ$ in preparation for the current work. Three grids were used (2.85×10^6 , 5.9×10^6 , and 10.0×10^6 cells) with a $\sqrt{2}$ difference in spacing near the body in each coordinate direction between successive grids. The fine grid DES predictions agreed with the database to within 5% of the lift, drag, and pitching moment – the expected uncertainty of the database. By examining pressure slices along the forebody, wing, and tail, it was determined that the coarse grid was sufficient to provide grid-independent pressures on the wing. The forebody and the tail, however, required the finest grid resolution. The grid spacing for the current effort was guided by these results. The coarse grid spacing was retained (roughly) on the wing, while the grid density was increased on the tail and forebody. The resulting full aircraft grid (both sides were modeled) resulted in a grid containing 6.5×10^6 cells – see Figures 7 and 8. The distance from solid surfaces to the first cell center normal to the wall was constant, resulting in an average distance in wall units

of 0.7. Cell growth in the wall-normal direction was specified using a geometric stretching factor of 1.25.

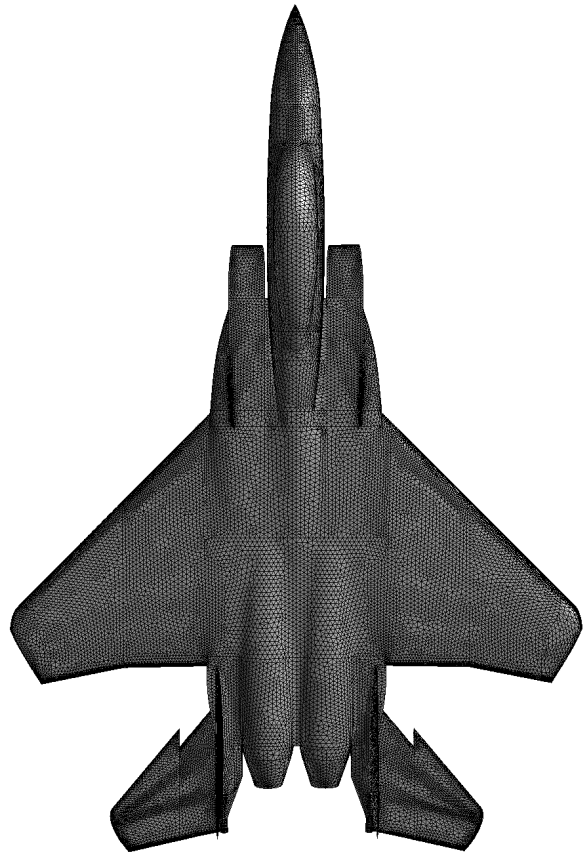


Fig. 7 Top view of the surface mesh on the F-15E.

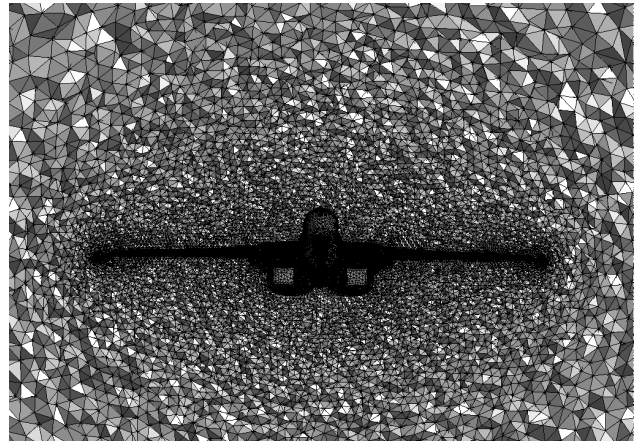


Fig. 8 Cutting plane showing the grid near the middle of the F-15E wing.

Previously,²⁵ the engine inlet and exhaust were set to a no-slip boundary condition. At an early phase of the study, modeling the inlet with a mass flow boundary condition was attempted. For the flow at 65° angle-of-attack, a separation bubble formed, which impinged on the inlet boundary. This in turn led to numerical instabilities since the flow was both entering and exiting a boundary at which a mass flow bound-

ary condition was being applied. For the current work, the inlet was extended downstream to allow the inflow boundary condition to the engine to be beyond the separation bubble created by the lower inlet lip (see Figure 9). The inflow boundary condition was set to specify the freestream static pressure. The engine outlet at the back of the aircraft was also set to freestream static pressure and the velocity set to the freestream value, but aligned with the longitudinal axis of the aircraft. Thus, the engine was roughly simulated to be at idle. This approach seems adequate since the thrust setting for the database was not specified.

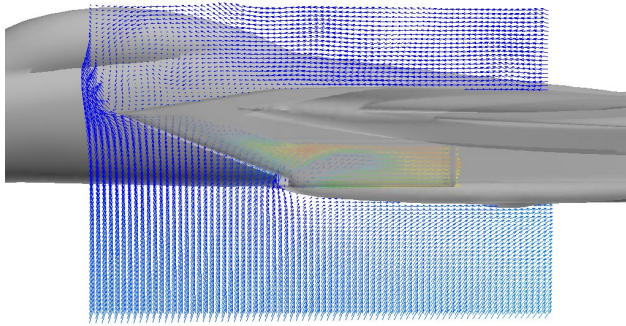


Fig. 9 Velocity vectors colored by x-velocity (along the aircraft’s longitudinal axis) on the centerline of the engine inlet. Outer wing panel has been made transparent to show the flow in the inlet.

As previously discussed, the F-15E has a non-zero yaw moment at $\alpha = 65^\circ$ and $\beta = 0^\circ$ due to asymmetric vortex shedding on the forebody due to small imperfections. This effect is crucial to predicting the spin since the induced yawing moment is a large factor in driving the motion. Wurtzler²¹ reproduced this effect computationally on an isolated F-15 forebody by adding a small bump on one side of the forebody above the midline and close to the front, the same approach is adopted in this work. Since the bump was only on one side of the aircraft, the full aircraft was gridded, rather than mirroring a half-aircraft model as possible on configurations with a symmetry plane. Surface pressures and streamlines are shown for an S-A RANS calculation in Figure 10. Despite the fact that the calculation was performed at zero sideslip, the vortices rapidly became asymmetric, causing a large difference in pressures on opposite sides of the forebody. This causes a significant yawing moment due to the long moment arm of the forebody. The bump is also visible on the blown up view in Figure 10 (on the right side, as the pilot sits). The pressures predicted are in qualitative agreement with previous computations and experiments²¹ shown in Figure 11 that were performed at a slightly lower angle of attack and for a laminar flow.

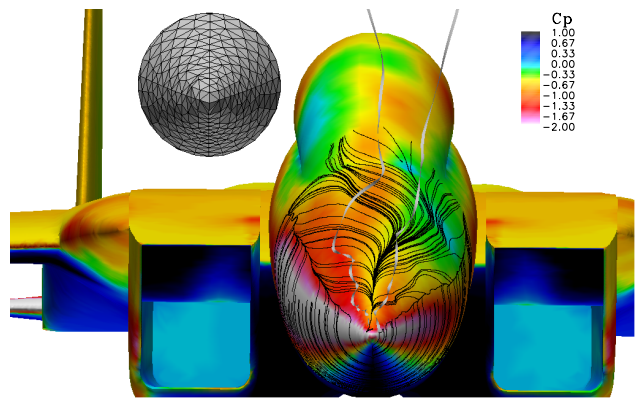


Fig. 10 View of the asymmetric vortex shedding on the F-15E at $\alpha = 65^\circ$ and no sideslip, SA RANS. Surface colored by pressure, surface streamlines in black, streamlines along vortex cores in grey. Zoomed view of the mesh on the forebody showing the bump on the right side (as the pilot sits).

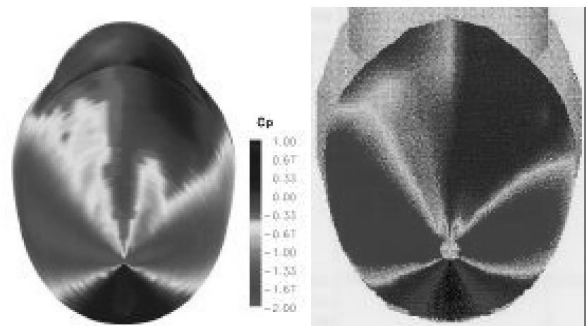


Fig. 11 Computed (left) and measured (right) pressure coefficients of the laminar flow over an isolated F-15 forebody at $\alpha = 62^\circ$.²¹

The static RANS cases were run with a maximum CFL of 1×10^6 to accelerate convergence to steady state. The DES static and the DES and RANS prescribed spins were calculated with a timestep of $0.7 \times 10^{-3} \text{sec}$ (0.014 non-dimensionalized by chord and freestream velocity). This value is sufficient for temporal resolution of the flowfield, based on the results of a previous timestep study.²⁵ Three Newton subiterations were used for the static cases, while five were employed for the prescribed spins. Time averages for the DES were acquired over 110 time units (8,000 timesteps).

Calculations were performed to match the specified spin: $M = 0.3$, $\alpha = 65^\circ$, $\beta = -2.5^\circ$, and a spin rate (Ω) of $100^\circ/\text{sec}$ about the velocity vector (0.124 non-dimensionalized by freestream velocity and half span). The freestream static pressure and temperature were specified from standard day conditions at 30,000ft. This resulted in a chord-based Reynolds number of 13.6×10^6 . The axis of rotation was determined by balancing the lift with the centripetal acceleration:²³

$$R = \left(\frac{1}{2m\Omega^2} \right) \rho U_\infty^2 S C_L \quad (9)$$

where R is the distance from the c.g. to the axis of rotation, m is the aircraft mass, and S is the reference area. The database C_L in the spin was used in this equation. The rotation axis was set to pass through the aircraft centerline, although it is likely that this is slightly in error since there was a small sideslip (see Pamadi²³ for a discussion on the location of the spin axis). Calculations were also performed with no spin (static) for comparison.

Results

Force coefficients for the spin and static cases, with comparison to the database, are shown in Table 2 at the end of the paper. Despite the fact that the RANS run with motion was performed time accurate, the forces converged to steady state values. Lift, drag, and pitching moment coefficients for the DES run are plotted against time in Figure 12, with the database values shown as the straight lines for reference. Side force (C_y), rolling moment (C_l), and yawing moment (C_n) coefficients are plotted in Figure 13.

Noticeable from the figure is that the difference in the database coefficients with and without spin are not large for lift, drag, and pitching moment. The lift and drag are expected to increase and the pitching moment decrease with the motion added. RANS predictions show the correct effect for lift and drag but the opposite effect for the pitching moment. DES predictions exhibit a slight decrease in lift and drag and an increase in pitching moment. One aspect also apparent from Figure 13 is that the differences in the force and moment coefficients from the static to spinning cases is not large, longer temporal samples are required to

resolve subtle changes in these quantities predicted in the DES.

The effect of the motion on the side force, rolling moment and yawing moment is shown in Figure 13 and Table 2. The yawing moment fails to decrease for DES, while a reduction is obtained in the RANS result. The rolling moment decreases for both simulation techniques, although the level of the difference is not as expected. Finally, the side force decreases for both RANS and DES under the spin, though less than expected. For both the static and spinning cases, the behavior of the forebody vortices likely has a dominant effect on these quantities. The forebody vortex is extremely sensitive to small disturbances, much of the error may be due to the inherent unpredictability of this phenomenon. Finally, it is also unknown if the quantities predicted from the database used precisely the same location for the spin axis.

Nevertheless, the accuracy of the lift, drag, and pitching moment coefficient for the DES with and without spin agree well with the database values, the worst disagreement being a 9% under-prediction of the drag. The effect of asymmetric yawing moment with no motion is well captured. RANS does fairly well also, with the worst disagreement being a 13% overprediction in lift. The surprising success of RANS on the static flow was shown and discussed previously.²⁵

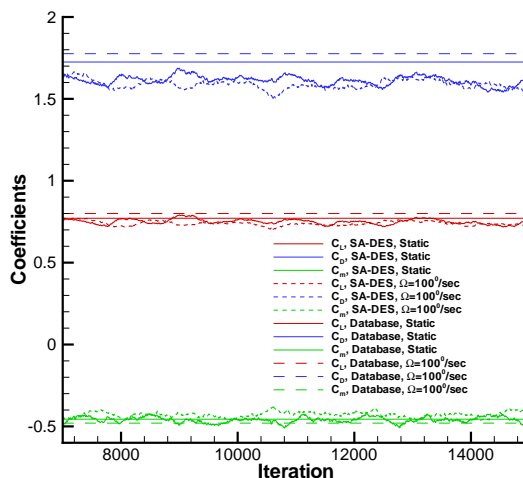


Fig. 12 Lift, drag, and pitching moment coefficients vs. time for SA-DES, static and spinning. Database¹ values represented by straight lines.

Summary

Detached-Eddy Simulation was used to predict the massively separated flow around a rectangular wing and around the F-15E statically, and with prescribed spinning motions. Assessment of accuracy was gauged by comparison to experimental data and comparison to RANS calculations.

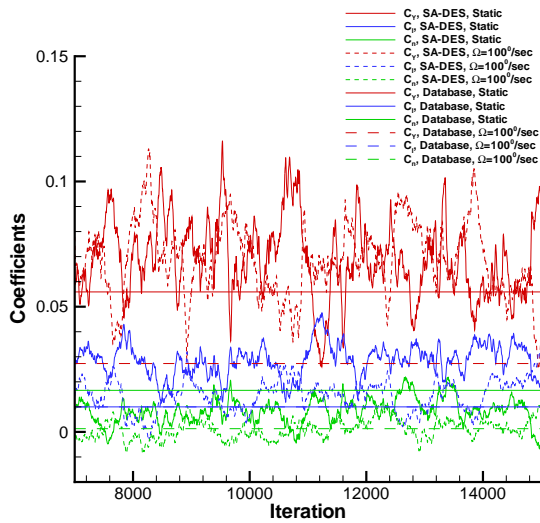


Fig. 13 Side force, rolling moment, and yawing moment coefficients vs. time for SA-DES, static and spinning. Database¹ values represented by straight lines.

For the rectangular wing, DES provided a more reasonable drag polar than RANS from the standpoint of predicting the limits of rotary stability using strip theory. However, the current DES calculations under-predicted lift near $C_{L_{max}}$. Future research will focus on improving the DES calculations in this range through adaptive mesh refinement. The wing was then given a prescribed spin at $\alpha = 24^\circ$ and a pro-spin rolling moment calculated. Thus the ability to predict autorotative effects on a wing using DES and grid motion was demonstrated qualitatively. Future efforts will apply a single degree-of-freedom model to enable prediction of the equilibrium rotation rates for stable autorotation, with comparisons made using the experiments of Knight.²⁰

A prescribed spin of the F-15E at 65° angle-of-attack was also calculated using RANS and DES. Predictions were assessed via comparison to Boeing's stability and control database.¹ The grid resolution was guided by previous computations,²⁵ and with the new grid, DES was able to accurately predict the static lift, drag, and pitching moment. The engine inlet was extended to enable setting inlet and outlet conditions to simulate the aerodynamic effect of the engines (at idle) on the airflow. Also, a small bump was added on one side of the grid to force the forebody vortex off symmetry, as would normally occur on the actual aircraft. The effect of the specified rotation on the force and moment coefficients in the stability and control database was subtle, and only qualitative agreement was achieved for some of these effects. However, the coefficients seemed reasonably accurate to motivate a six degree-of-freedom calculation in the near future.

Acknowledgements

The authors gratefully acknowledge the support of AFOSR Grant F49620-00-1-0050 (Program Manager: Dr. Tom Beutner). The authors are also grateful for the assistance of Glen Peters, Dr. Ken Walck, and Dr. Walt Labozzetta of Boeing Military, who provided the stability and control database and the F-15E geometry. Finally, the project would not have been possible without the support and cpu hours at the ASC MSRC and Maui HPCC.

References

- ¹Peters, G. and Walck, K., "Excerpts from the F-15E Stability and Control Database", *Personal Communication*, Dec. 2000.
- ²Spalart, P.R., Jou, W.H., Strelets, M. and Allmaras, S.R., 1997, "Comments on the Feasibility of LES for Wings, and on a Hybrid RANS/LES Approach," *First AFOSR International Conference on DNS/LES*, Ruston, Louisiana, USA.
- ³Strang, W.Z., Tomaro, R.F, Grismer, M.J., 1999, "The Defining Methods of Cobalt60: a Parallel, Implicit, Unstructured Euler/Navier-Stokes Flow Solver," *AIAA 99-0786*, January 1999.
- ⁴Grismer, M. J., Strang, W. Z., Tomaro, R. F. and Witzemman, F. C., "Cobalt: A Parallel, Implicit, Unstructured Euler/Navier-Stokes Solver," *Advances in Engineering Software*, Vol. 29, No. 3-6, pp. 365—373, 1998.
- ⁵Tomaro, R.F., Strang, W.Z., and Sankar, L.N., 1997, "An Implicit Algorithm for Solving Time Dependent Flows on Unstructured Grids," *AIAA 97-0333*, January 1997.
- ⁶Spalart, P.R. and Allmaras, S.R., 1994, "A One-Equation Turbulence Model for Aerodynamic Flows," *La Recherche Aeronautique* 1, pp. 5-21.
- ⁷Spalart, P.R. (2000), "Strategies for Turbulence Modeling and Simulations", *International Journal of Heat and Fluid Flow*, 21, p. 252-263.
- ⁸Shur, M., Spalart, P. R., Strelets, M., and Travin, A, 1999, "Detached-Eddy Simulation of an Airfoil at High Angle of Attack", 4th Int. Symp. Eng. Turb. Modelling and Measurements, Corsica, May 24-26, 1999.
- ⁹Gottlieb, J.J. and Groth, C.P.T., 1988, "Assessment of Riemann Solvers for Unsteady One-Dimensional Inviscid Flows of Perfect Gases", *Journal of Computational Physics*, 78, pp. 437-458.
- ¹⁰Karypis, G., Schloegel, K. and Kumar, V., 1997, "ParMETIS: Parallel Graph Partitioning and Sparse Matrix Ordering Library Version 1.0", University of Minnesota, Department of Computer Science, Minneapolis, MN 55455, July 1997.
- ¹¹Squires, K.D., Forsythe, J.R. Spalart, P.R., 2001, "Detached-Eddy Simulation of the separated flow around a forebody cross-section", *Direct and Large-Eddy Simulation IV*, ERCOFTAC Series - Volume 8, B.J. Geurts, R. Friedrich and O. Metais, editors, Kluwer Academic Press, pp. 481-500.
- ¹²Kotapati-Apparao, R., Forsythe, J., Squires, K., "Computation of the Flow Over a Maneuvering Spheroid," *AIAA 2003-0269*, Jan 2003.
- ¹³Viswanathan, A., Klismith, K., Forsythe, J., Squires, K., "Detached-Eddy Simulation Around a Rotating Forebody," *AIAA 2003-0263*, Jan 2003.
- ¹⁴Forsythe, J.R., Hoffmann, K.A., Dieteker, F.-F., "Detached-Eddy Simulation of a Supersonic Axisymmetric Base Flow with an Unstructured Flow Solver," *AIAA 00-2410*, June 2000.
- ¹⁵Pirzadeh, S., 1996, "Three-dimensional Unstructured Viscous Grids by the Advancing Layers Method," *AIAA Journal*, 34, pp. 43-49.

¹⁶Spalart, P., “Young-Person’s Guide to Detached-Eddy Simulation Grids,” *NASA CR 2001-211032*.

¹⁷Travin, A., Shur, M., Strelets, M. and Spalart, P.R. (2000), “Detached-eddy simulations past a circular cylinder”, *Flow, Turbulence, and Combustion*, **63**, pp. 293-313.

¹⁸Wurtzler, K.E., “An Effectiveness Study of F-15 Forebody Flow Analysis Using Cobalt,” *AIAA Paper 99-0536*, January 1999.

¹⁹Constantinescu, G.S. and Squires, K.D., 2000, “LES and DES investigations of turbulent flow over a sphere”, *AIAA Paper 2000-0540*.

²⁰Knight, M., “Wind Tunnel Tests on Autorotation and the ‘Flat Spin’,” NACA Report No. 273, 1927.

²¹Wurtzler, K.E., “An Effectiveness Study of F-15 Forebody Flow Analysis Using *Cobalt*₆₀,” *AIAA 99-0536*, 1999.

²²Pauley, H., Ralston, J., and Dickes, E., “Experimental Study of the Effects of Reynolds number on high Angle of Attack Aerodynamic Characteristics of Forebodies during rotary motion,” *NASA CR 195033*, Jan. 1995.

²³Pamadi, B.N., Performance, Stability, Dynamics, and Control of Airplanes, AIAA Education Series, pp. 627–672, 1998.

²⁴Forsythe, J.R., Woodson, S.H., “Unsteady CFD Calculations of Abrupt Wing Stall Using Detached-Eddy Simulation,” *AIAA 2003-0594*, Jan 2003.

²⁵Forsythe, J.R., Squires, K.D., Wurtzler, K.E., Spalart, P.R., “Detached-Eddy Simulation of Fighter Aircraft at High Alpha,” *AIAA 2002-0586*, Jan 2002.

		C_L	C_D	C_Y	C_l	C_m	C_n
Static	Database ¹	0.77	1.725	0.056	0.010	-0.46	0.017
	SA DES	0.75	1.61	0.069	0.029	-0.46	0.0084
	SA RANS	0.87	1.86	0.060	0.036	-0.51	0.0093
Spinning	Database ¹	0.80	1.776	0.0273	0.0099	-0.48	0.0013
	SA DES	0.74	1.59	0.067	0.015	-0.43	0.0084
	SA RANS	0.90	1.91	0.051	0.021	-0.49	0.0015

Table 2 Static and spinning force and moment coefficients of the F-15E at $\alpha = 65^\circ$, $\beta = -2.5^\circ$, and $\Omega = 100^\circ/s$